Continuity within the somatosensory cortical map facilitates learning

Henri Lassagne, Dorian Goueytes, Daniel Shulz, Luc Estebanez, Valérie Ego-Stengel

Report

Cell Reports

Continuity within the somatosensory cortical map facilitates learning

Graphical abstract

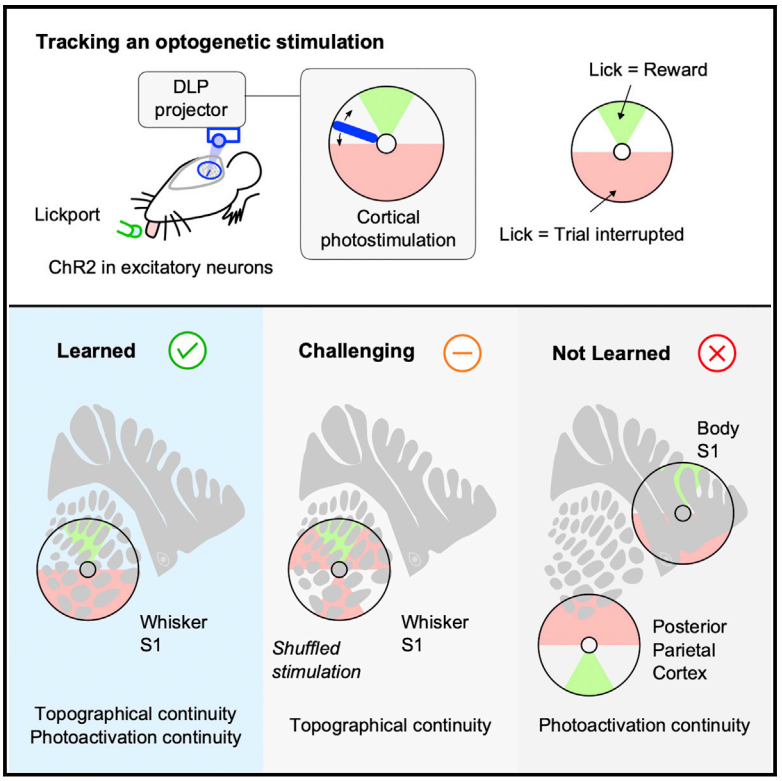

Highlights

- Mice accurately track an optogenetic stimulation bar over the cortical surface
- Continuity of the cortical area's topography is critical for learning
- Spatiotemporal continuity of the photoactivation trajectory supports learning
- This study demonstrates the functional role of continuity in cortical maps

Authors

Henri Lassagne, Dorian Goueytes, Daniel E. Shulz, Luc Estebanez, Valerie Ego-Stengel

Correspondence

valerie.ego-stengel@cnrs.fr

In brief

Lassagne et al. design a mesoscale optogenetic discrimination task in mice targeting several cortical areas. Mice become experts at tracking the rotating photostimulation bar but only when both the photostimulation trajectory and the cortical map topography are continuous.

Lassagne et al., 2022, Cell Reports *39*, 110617
April 5, 2022
https://doi.org/10.1016/j.celrep.2022.110617

CellPress

Cell Reports

CellPress
OPEN ACCESS

Report

Continuity within the somatosensory cortical map facilitates learning

Henri Lassagne,[1] Dorian Goueytes,[1] Daniel E. Shulz,[1] Luc Estebanez,[1,2] and Valerie Ego-Stengel[1,2,3,*]
[1]Université Paris-Saclay, CNRS, Institut des Neurosciences Paris-Saclay, 91400 Saclay, France
[2]These authors contributed equally
[3]Lead contact
*Correspondence: valerie.ego-stengel@cnrs.fr
https://doi.org/10.1016/j.celrep.2022.110617

SUMMARY

The topographic organization is a prominent feature of sensory cortices, but its functional role remains controversial. Particularly, it is not well determined how integration of activity within a cortical area depends on its topography during sensory-guided behavior. Here, we train mice expressing channelrhodopsin in excitatory neurons to track a photostimulation bar that rotated smoothly over the topographic whisker representation of the primary somatosensory cortex. Mice learn to discriminate angular positions of the light bar to obtain a reward. They fail not only when the spatiotemporal continuity of the photostimulation is disrupted in this area but also when cortical areas displaying map discontinuities, such as the trunk and legs, or areas without topographic map, such as the posterior parietal cortex, are photostimulated. In contrast, when cortical topographic continuity enables to predict future sensory activation, mice demonstrate anticipation of reward availability. These findings could be helpful for optimizing feedback while designing cortical neuroprostheses.

INTRODUCTION

Primary sensory areas of the neocortex are involved in sensory perception of several modalities. For example, microstimulations of specific areas of the cortex in humans produce vivid visual, tactile, or auditory percepts (Dobelle et al., 1974; Penfield and Boldrey, 1937; Penfield and Rasmussen, 1950; Schmidt et al., 1996).

These sensory areas are organized topographically with respect to the periphery (Daniel and Whitteridge, 1961; Merzenich et al., 1975; Penfield and Boldrey, 1937). In the primary somatosensory cortex (S1), Penfield and collaborators have shown that neighboring cortical zones encode information from neighboring patches of skin on the body (Penfield and Boldrey, 1937). Such cortical representation of the body surface in S1 is a common feature of mammals. In rodents, the whiskers' follicles on the snout are connected to distinct clusters of cells within S1, called barrels (Woolsey and Van der Loos, 1970), that retain the spatial organization of the follicles.

One question concerns to what extent activation of neuronal ensembles in the cortical maps is necessary and sufficient for eliciting percepts that can drive behavior (Ceballo et al., 2019a; Chen et al., 2020; Dalgleish et al., 2020). Animals can be trained to report direct cortical stimulation of primary sensory areas for all modalities (Ceballo et al., 2019a; Chen et al., 2020; Choi et al., 2011; Houweling and Brecht, 2008; Huber et al., 2008; Peng et al., 2015). Interestingly, several studies have shown that animals trained in a localized sensory perception task could rapidly generalize when the peripheral stimuli were replaced by cortical microstimulations (Chen et al., 2020; Leal-Campanario et al., 2006; O'Connor et al., 2013; Peng et al., 2015; Romo et al., 1998; Sachidhanandam et al., 2013; Tabot et al., 2013; Venkatraman and Carmena, 2011). This seemingly immediate interchangeability of natural and artificial stimuli strongly supports a prominent role of cortical activity in sensory perception. Stimulation of distinct cortical zones in a topographic sensory map elicited localized percepts matching the expected peripheral locations on the sensory organ (Bosking et al., 2017; Ceballo et al., 2019a; Chen et al., 2020; Flesher et al., 2016; Winawer and Parvizi, 2016). This result has been interpreted as additional evidence that the topographical organization of sensory areas serves a fundamental function for sensory processing (Harding-Forrester and Feldman, 2018; Kaas, 1997). However, there is no direct evidence that cortical topography is important for brain function. On the contrary, it has been suggested that topography could be a mere consequence of the way cortical areas form early in development. In this alternative view, the spatial arrangement of cortical zones as an orderly mosaic may have no functional impact on the computations performed by the cortex (Lashley, 1939). To solve this controversy, it becomes necessary to directly manipulate cortical activity at the scale of the topographic organization of the cortex, and test its causal impact on behavior.

Almost all studies linking cortical activity and perception have focused on single-stimulus detection, or discrimination between a few stimuli each presented individually. However, more complex stimuli in which information is spatially and temporally distributed are more likely to engage the computational capacity

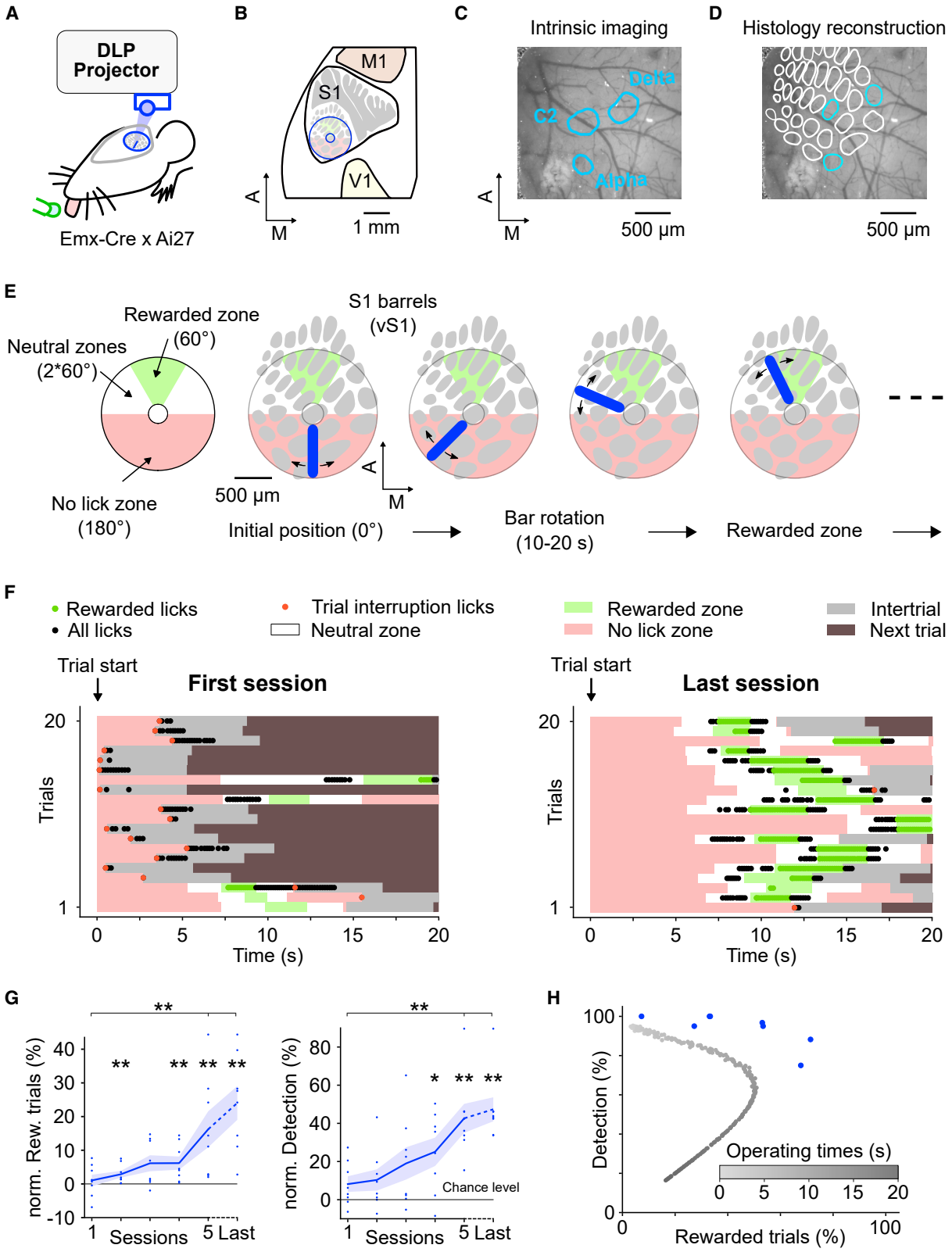

(legend on next page)

of the cortical network. Indeed, at the microcircuit level, functional topography is known to be intrinsically associated with precise intracortical connectivity diagrams (Jiang et al., 2015; Narayanan et al., 2015; Rockland et al., 1982). These highly non-random connections result in differential sensory processing, depending on the spatiotemporal sequences of neurons being activated. Notably, the cortex seems particularly useful to differentially integrate multiple sensory inputs over time, via nonlinear transformations (Estebanez et al., 2018; Nogueira et al., 2021).

To test the role of topography in cortical function, two different types of mesoscopic patterns should thus be contrasted: on the one hand, topographic patterns that match the cortical activation patterns known to occur following peripheral stimulation, and on the other hand, non-topographic patterns that do not match expected cortical activation, for example because they correspond to synchronous stimulation of distant peripheral zones that do not normally occur. Our underlying hypothesis in contrasting such patterns is that they should result in different cortical processing because of the detailed structure of the cortical network.

We carried these tests by causally manipulating the activity of cortical neurons in transgenic mice, using dynamical patterns of optogenetic activation. By design, the behavior of the mouse could only be due to perception of cortical activity. We applied a continuously moving stimulus projected onto different cortical areas: the primary somatosensory cortex (vS1), known for its orderly two-dimensional topography; the trunk and legs area primary somatosensory area (bS1), which contains discontinuities in its topography; and the posterior parietal cortex (PPC), which lacks a clear topography. Our results point to differential sensory processing in topographic and non-topographic areas.

RESULTS

Mice learn the angular position of a rotating optogenetic stimulus projected onto the barrel cortex

In this study, we tested whether head-fixed, water-restricted mice expressing channelrhodopsin in excitatory cortical neurons could actively track the position of a photostimulation applied on vS1 (Figures 1A and 1B). We first determined the location of at least three barrels, including the C2 barrel, by intrinsic imaging (Figure 1C). The locations were confirmed postmortem by histological barrel map reconstruction (Figures 1D (Perronnet et al., 2016)). We then projected a rotating bar of light inside a disk centered on the C2 barrel (Figure 1E). The light bar turned smoothly and differently for each trial, activating sequentially contiguous zones of the barrel cortex (Figure S1). Mice could obtain reward by licking when the photostimulation bar was within a specific rewarded zone (Figure 1E). Licking when the bar was in the no-lick zone immediately ended the trial and started a 5-s intertrial interval without stimulation.

In Figure 1F, the first 20 consecutive trials are shown for the first and 10th session for one mouse. During the first session, the mouse licked randomly, which often cancelled the trial. During the 10th session, the mouse successfully refrained from licking in the no-lick zone, until approaching the rewarded zone. All eight trained mice learned the task in 5 days (Figure 1G). Rewarded trials increased on average by over 15% (Figure 1G left, Wilcoxon test, $p = 0.0078$), while the detection level, calculated only on trials with available reward, increased up to 40% above chance level (Figure 1G right, Wilcoxon test, $p = 0.0078$). This corresponded to over 90% of detection calculated on all trials (Figure S2). Taken together, these learning curves suggest that all mice learned both to locate which sector of the stimulated cortical area leads to reward availability and to refrain from licking in the no-lick zone in order to increase the total number of rewarded trials. Three mice out of eight were trained for more than 5 days, and population analysis on the last sessions pooled across all mice showed that performance continued to increase (Figure 1G, "last").

We were concerned that the mice might learn the average timing from the onset of the trial to the entrance in the rewarded zone, without relying on the angular position of the photostimulation. Thus, we designed an algorithm that solves the task using only time cues. The results from this algorithm are shown in Figure 1H for all possible times of onsets of licks (operating times). As expected, at short operating times (light gray points), most licks fell in the no-lick zone, which in turn resulted in very low numbers of rewarded trials. The longest operating times (dark gray points) led to late lick onsets, which missed the rewarded zones. All mice demonstrated higher performance than any version of the temporal algorithm (Wilcoxon, $p = 0.0078$). Thus, mice did indeed use the spatial location of the stimulation to guide licking, and not only temporal cues.

To further investigate spatial learning, we analyzed the radial distribution of the photostimulation angle for all lick times before and after learning (Figure 2A top, same sessions as in Figure 1F; see also Figure S3). The proportion of licks for the rewarded zone increased with training from 19% to 61%, while the proportion of

Figure 1. Mice were trained to lick for rewards when a moving photostimulation bar entered a defined vS1 zone

(A) Sensory-guided licking task. A digital projector sends frames through an optical window. A water tube detects licks and delivers rewards when appropriate.

(B) Location of the stimulation disk over vS1 (cortical map adapted from Knutsen et al., 2016, and Vanni et al., 2017).

(C) Contours of the intrinsic imaging responses for individual deflection of whiskers Alpha, C2, and Delta overlaid on surface blood vessels.

(D) Histological reconstruction of the barrel map for the experiment in (C).

(E) When the bar was in the green zone, licks were rewarded. In the red zone, a lick ended the trial. In the white zones, licks were ignored. Right: snapshots from one trial.

(F) Raster plots of licks (dots) during 20 consecutive trials in the first and 10th session for one mouse.

(G) Average learning curves (± SEM, n = 8 mice) quantified by the detection level and the percentage of rewarded trials, normalized by subtracting the chance level (see STAR Methods). Data are presented for the first five sessions and the last session of training for each mouse, regardless of the number of trained sessions. Wilcoxon tests, *$p < 0.05$, **$p < 0.01$.

(H) Performance curve of an algorithm solving the task with a pure temporal strategy (see STAR Methods). Each gray dot is the performance of the algorithm triggering licks at a specific time, the operating time (grayscale), across all 252 possible trials. Blue dots are the mice performance on their last session.

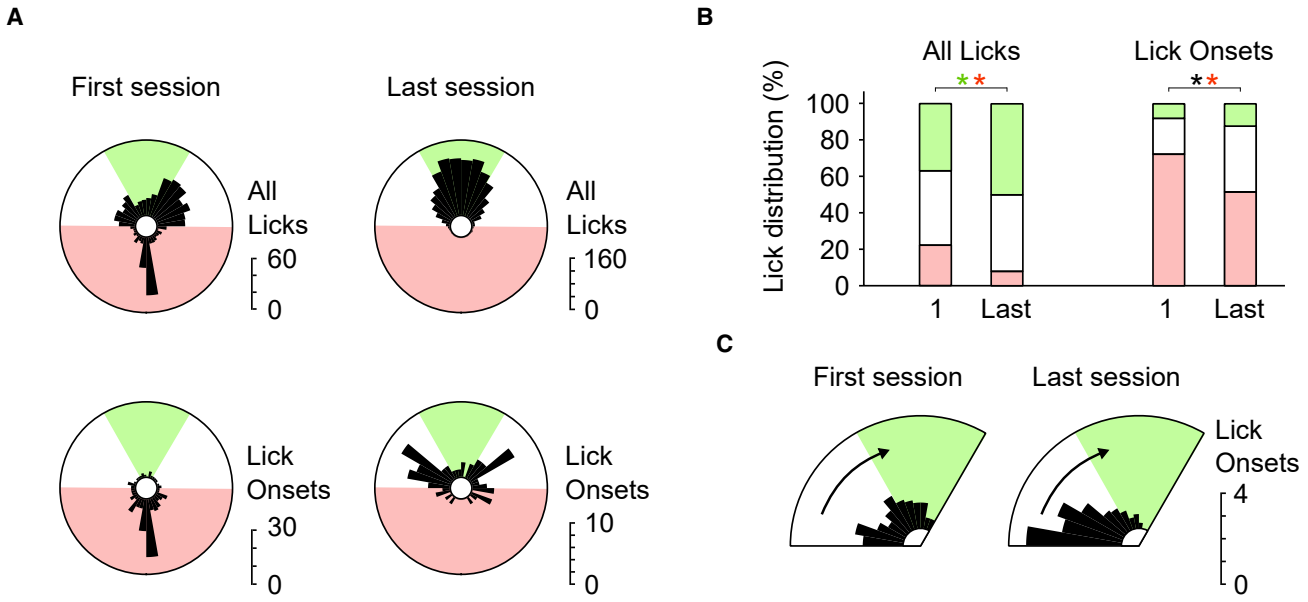

Figure 2. Redistribution of the angular positions of the optogenetic bar at lick times shows spatial anticipation of the reward

(A) Spatial distribution of the optogenetic stimulus angle for all licks (top) and lick onsets (bottom), for the sessions from Figure 1F.

(B) Average distribution of all licks and lick onsets for which the optogenetic bar was in the rewarded, no-lick, and neutral zones for the first and last session (n = 8). One-sided Wilcoxon tests, *p < 0.05, colors match the zones (black = neutral zone).

(C) Average spatial distribution of the stimulus angle for lick onsets in the neutral and rewarded zones. Trials entering from the right were symmetrized before averaging. Only the first 20 rewarded trials of a given session were used for this analysis, ensuring that the mice were highly motivated.

licks for the no-lick zone decreased from 26% to 1%. Interestingly, after learning, lick onsets occurred mainly for the zones flanking the rewarded zone (Figure 2A, bottom). This suggests that the mouse started licking after the bar left the no-lick zone, even before entering the rewarded zone. Population analysis confirmed this redistribution of licks and lick onsets across cortical photostimulation zones (Figure 2B, n = 8 mice, Wilcoxon tests, *p < 0.05) and specifically right after entry in the neutral zone (Figure 2C).

After learning the task, three mice were trained for a further 5 days with a more challenging, extended no-lick zone (Figure S4). The high performance and increased alignment of lick onsets to the no-lick/neutral zones border further demonstrates the fine readout resolution attained (Figures 2C and S4G).

Mice use the spatial continuity of the stimulation space to solve the task

To check if the anticipatory licking shown in Figure 2C is based on spatial rather than temporal cues, we trained three naive mice in a shuffled condition (Figure 3A; see STAR Methods). Across the 10 sessions of training, the percentage of rewarded trials did not increase significantly, remaining far below values reached in the standard condition (Figure 3B, Mann-Whitney [MW] test; p = 0.018). Nonetheless, two out of three mice reached a 100% detection level after 10 days. These results suggest that the spatial discontinuities reduced the proportion of successful trials, but that mice could still learn the rewarded zone location as much as in the standard condition. Interestingly, when we looked at the time course of successful trials, we found that mice strategy differed from that in the standard task: they started licking only when the optogenetic bar reached the rewarded zone, instead of anticipating its entry (example in Figures 3C versus 2F). We quantified this observation by measuring the delay between lick onset and entry in the rewarded zone. In the standard condition, mice anticipated the rewarded zone entry by a median of ~1 s, in contrast to the ~300-ms delay in the shuffled condition (Figure 3D), and the absence of licks in the neutral zone just preceding the rewarded zone (Figure 3E). Anticipation of the rewarded zone eventually emerged after an additional 3 days of training (Figure 3D).

We wondered whether mice that had already learned the task in the standard condition could easily adapt to the shuffled condition. Three expert mice in the standard condition were tested in the shuffled condition. Despite a drop in performance, these mice remained experts at detecting the rewarded zone (100% detection level) but stopped anticipatory licking (Figure 3F, p < 0.0001), demonstrating again a direct effect of the spatial continuity of trajectories on behavior.

To summarize, these results suggest that, in order to track the cortical optogenetic bar and predict its trajectory, mice exploit the spatial continuity of cortical stimulation.

Learning is disrupted by discontinuities in the cortical map

To further test this finding, we asked if discontinuities in the targeted cortical map itself might also affect learning. We trained naive mice to learn the same task while centering the photostimulation outside of the barrel cortex. First, we selected a cortical

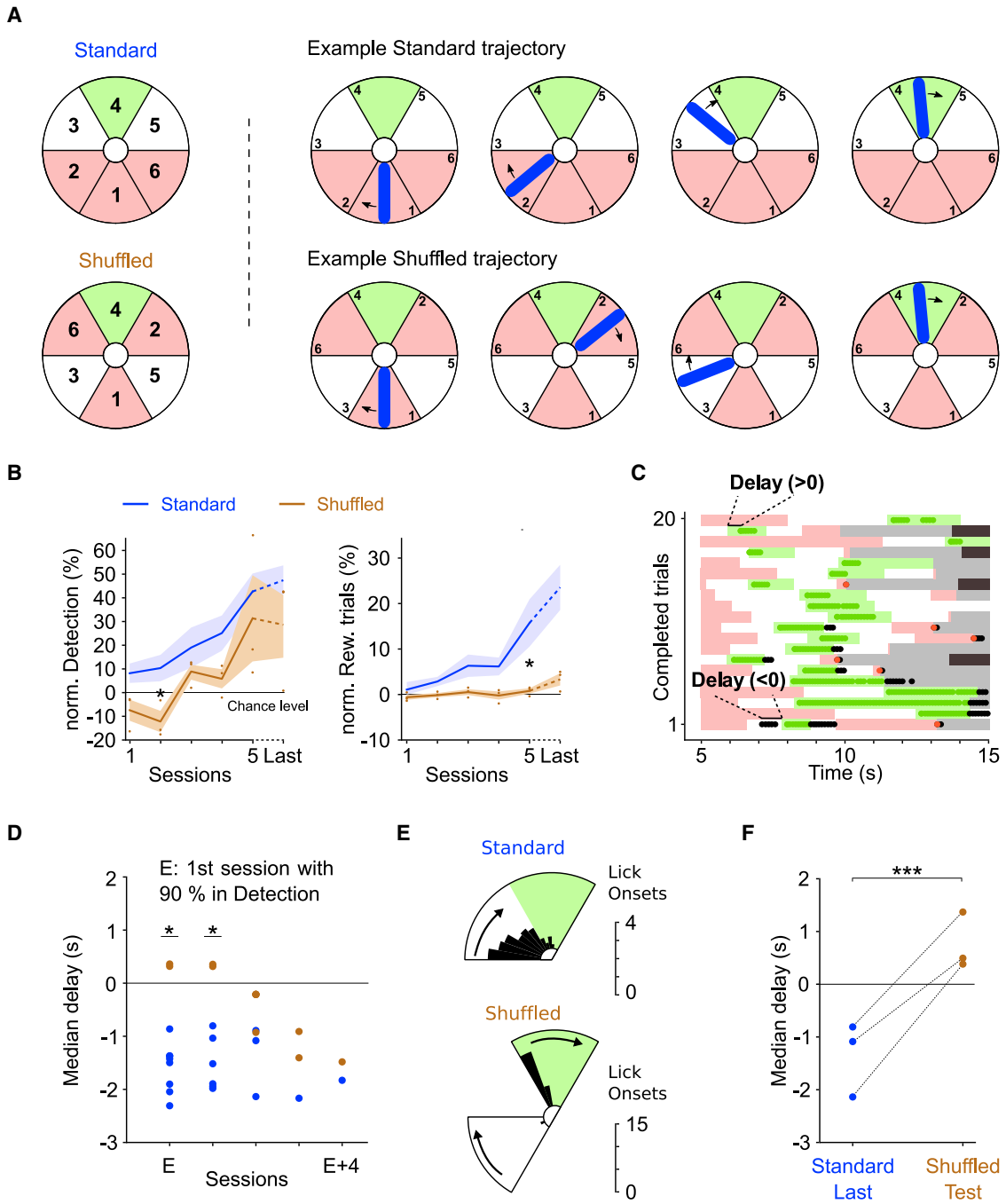

Figure 3. Mice rely on the spatial continuity of the stimulated area to learn the task

(A) Left, reorganization of angular sectors of the stimulation disk from the standard condition (top) to the shuffled condition (bottom). Sectors 1 and 4 are unchanged; other sectors are permuted. Right, example snapshots of the same trajectory in both conditions. As several sectors are swapped, the stimulation bar jumps from one sector to another, but stays in the no-lick, neutral, and rewarded zones following exactly the same timeline as in the standard condition.

(B) Average learning curves (± SEM) for the standard (blue, n = 8) and shuffled (brown, n = 3) conditions. Two-sided MW test, *p < 0.05.

(C) Raster plot of 20 consecutive completed trials for a mouse trained in the shuffled condition, for the first session with a high (>90%) detection level (session 6). Delay is the time from entry in the rewarded zone to first reward.

(D) Median delay for the standard (blue) and shuffled (brown) conditions. For each mouse, session E is the first session with a detection level above 90%. Only consecutive sessions with a detection rate of 90% or more are shown. One-sided MW test, *p < 0.05.

(E) Average spatial distributions of stimulus angle for lick onsets for rewarded trials (as in Figure 2C), for standard and shuffled conditions in session E + 1.

(F) Median delay for the last session in the standard condition, and for a test session in the shuffled condition 1 day later (n = 3 mice). One-sided MW calculated for each mouse, ***p < 0.001.

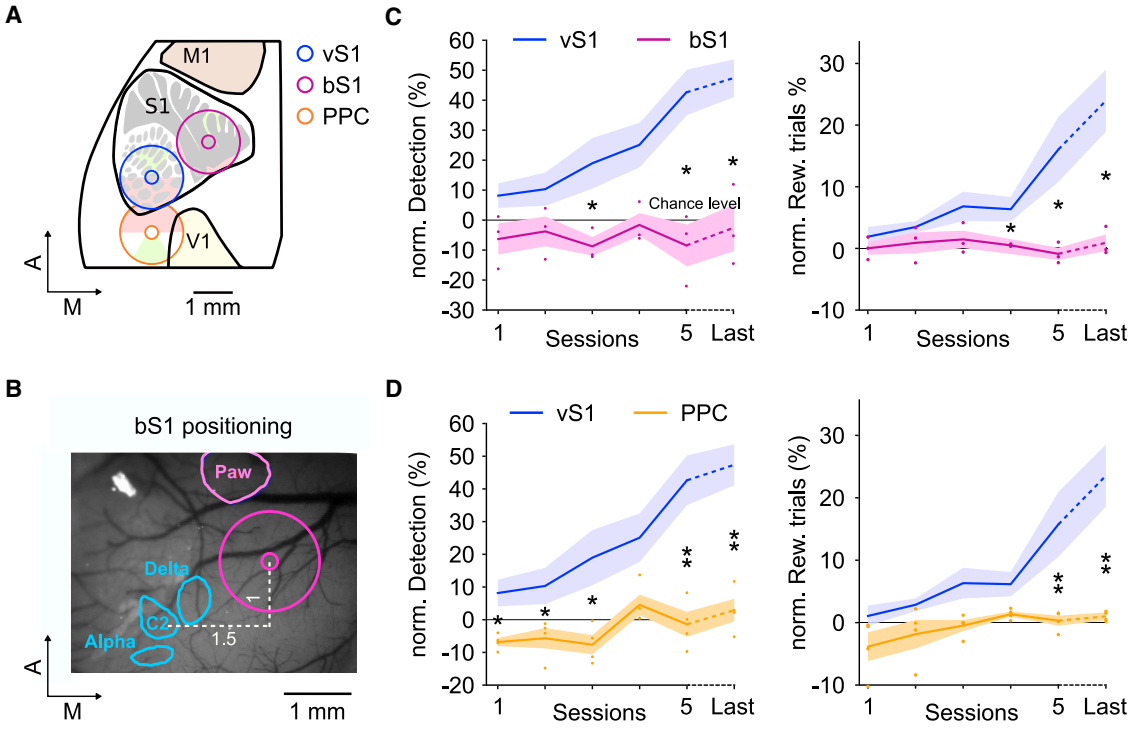

Figure 4. Learning is only possible in a cortical area that contains a continuous topographic representation

(A) Stimulation disks including rewarded/no-lick zones on vS1 (blue), bS1 (magenta), and PPC (orange).

(B) Contours of the intrinsic imaging responses for individual deflection of whiskers Alpha, C2, and Delta (blue), and for mechanical vibration on the paw (pink), overlaid on surface blood vessels. Magenta, stimulation disk on bS1.

(C) Average learning curves (± SEM) for stimulation of vS1 (blue, n = 8) and bS1 (magenta, n = 3).

(D) Same as C for PPC (orange, n = 4). In two mice, PPC training followed vS1 training. This might explain the significant differences in detection observed in the first session. (C, D) Two-sided MW, *p < 0.05, **p < 0.01.

area (bS1) where the adjacent trunk, limb, and snout representations resulted in discontinuities in the cortical map (Figures 4A and 4B). None of the mice reached performance comparable with mice trained with photostimulation on vS1 (Figure 4C; MW test on the last sessions; rewarded trials, p = 0.032; detection, p = 0.019). Second, we centered the stimulation on PPC in four mice already trained on vS1. The rationale was to select a non-primary sensory area, for which topography is not a strong organizing principle. Similar to mice trained on bS1, these mice did not learn the task (Figure 4D; rewarded trials, p = 0.008; detection, p = 0.008 compared with vS1 mice). This difference in performance could not be due to a lack of induced activity: we recorded electrophysiological activity while projecting patterns of light on the cranial window and found reliable activity induced by photostimulation, regardless of the electrode position (Figure S1). Together, these results suggest that the continuous topography present in vS1 is necessary for learning the optogenetically mediated task.

DISCUSSION

We have shown that mice can learn to use patterned cortical stimulations as dynamical cues to guide their behavior. Learning only occurred when the stimulus was continuous across space and time, and when the target area included a continuous topographic map of the sensory periphery. Our findings thus fit with the general idea that the topography of a cortical area shapes input integration in neuronal networks.

Mesoscopic cortical patterns causally drive behavior

In order to activate the cortical surface with high-resolution dynamical patterns, we chose to use optogenetic stimulation, which activates predominantly upper layers (Yizhar et al., 2011). The dense horizontal intracortical connectivity in these layers supports continuous propagating waves of depolarization at a mesoscopic scale (Muller et al., 2018; Vilarchao et al., 2018). The fact that mice were able to lick in response to supragranular mesoscopic patterns is direct evidence that patterns at that scale can indeed acquire functional relevance for perception and behavior.

Mice learn the optogenetic task similarly to a sensory go/no-go task

During learning, mice first improved their task performance by licking when the optogenetic bar entered the rewarded zone. In parallel, many trials were still aborted because of licks in the no-lick zone. This asymmetric learning for rewarded and non-rewarded trials is similar to the dynamics described in a classic go/no-go sensory discrimination task (Bathellier et al., 2013). Interestingly, the delay between optogenetic stimulation and lick

response was comparable with reaction times following peripheral stimulation, ~300 ms (Figure 3) (Abbasi et al., 2018; Ceballo et al., 2019b; El-Boustani et al., 2020; Huber et al., 2008; Sachidhanandam et al., 2013). Thus, mice integrate cortical stimuli similarly to peripheral stimuli into perception and behavior.

Breaking spatiotemporal continuity disrupts learning

We tested two different ways of disrupting the continuity of optogenetic perception. First, we manipulated the spatiotemporal parameters of the cortical stimulus by shuffling spatial zones of the stimulated area. Second, we applied stimulation on an area in which topography is discontinuous, such as bS1. In both cases, learning was severely impaired (Figures 3 and 4). In bS1, this could be due to the fact that the optogenetic bar crosses cortical zones that correspond to non-contiguous peripheral skin zones. Thus, the stimulation could be perceived as a stimulus jumping between many different locations; for example, jumping from limbs to trunk. If, as proposed, S1 serves as a body model to simulate and predict ongoing behavior (Brecht, 2017), the induced S1 activity could indeed be difficult to read out. Continuity of activity in a topographic area would then be critical for sensorimotor anticipation and learning.

Biomimetism facilitates neuroprosthetic learning

Beyond a better understanding of sensory perception, our findings could be key to the efficient delivery of sensory information in the context of sensorimotor neuroprostheses (Chen et al., 2020; Dadarlat et al., 2015; Hartmann et al., 2016; O'Doherty et al., 2011). Recent active neuroprostheses tend to match as closely as possible the spatial and temporal aspects of physiological cortical responses to tactile and proprioceptive inputs (Flesher et al., 2021; Tabot et al., 2015), as well as to visual inputs (Dobelle, 2000; Fernández et al., 2021). However, most studies relied on discrete patterns of stimulation in space and time, whereas everyday prosthesis use is likely to generate complex, continuous sensory feedback. Here, we have designed a class of spatially and temporally continuous feedback at the cortical surface. Although this remains a partial biomimetic activation, it shares some features of known cortical activity patterns, notably the propagation of cortical waves of activation (Muller et al., 2018). In our study, such stimulation of a topographically organized sensory cortex could be integrated with a high degree of spatial precision into behavior, including anticipatory processes that could promote dexterous movements of a closed-loop neuroprosthesis.

Longer-timescale reorganization of the cortex during learning

With additional training, learning the disrupted conditions may eventually occur. For example, the activity patterns evoked in S1 in the shuffled condition share features with those following the surgical rotation of a skin flap while keeping nerve fibers intact (Rosselet et al., 2008). In those experiments, cortical topography was remodeled over the course of 2 weeks, so that a new somatosensory map emerged, matching perfectly the new contiguity of peripheral skin zones. Both maps then co-existed, suggesting that several readout schemes can be implemented simultaneously in a cortical area. In our experiments, a reorganization of spatial readout mechanisms by downstream areas could still be at play. The extent of such reorganization during neuroprosthesis use has been debated (Makin and Bensmaia, 2017). Recent studies on participants using a sensorimotor bionic arm suggest that long-term perceptual alignment of the prosthesis and the missing limb requires that sensor location and the connected nerve sensation should roughly match (Cuberovic et al., 2019; Ortiz-Catalan et al., 2020; Schofield et al., 2020). Thus, remapping in adults may occur, but only to a certain degree (Tabot et al., 2015).

Limitations of the study

In this study, we targeted several cortical areas to explore how mice can efficiently read out patterns of neural activation. While their different topographical arrangement can explain our results, these cortical areas may differ in additional ways, including the level of expression of the ChR2 transgene. However, transgene expression appears similar across the neocortex of our mouse line, as detailed histological sections generated for the Allen Brain Atlas show (Madisen et al., 2012). We further checked that, in our experimental conditions, optogenetic stimulation evoked reliable spiking activity (Figures S1D and S1E). Similar activation has been reported in primary auditory cortex using the same mouse line (Ceballo et al., 2019b). We are therefore confident that the photostimulation pattern activated the cortex adequately in all our experimental conditions. Another concern is that these areas project to different brain regions, which might affect the behavioral output during the task. Further experiments will be necessary to explore this hypothesis.

STAR★METHODS

Detailed methods are provided in the online version of this paper and include the following:

- KEY RESOURCES TABLE
- RESOURCE AVAILABILITY
  - Lead contact
  - Materials availability
  - Data and code availability
- EXPERIMENTAL MODEL AND SUBJECT DETAILS
- METHOD DETAILS
  - Mouse preparation
  - Optogenetic photostimulation
  - Behavioral training
  - Histology
- QUANTIFICATION AND STATISTICAL ANALYSIS

SUPPLEMENTAL INFORMATION

Supplemental information can be found online at https://doi.org/10.1016/j.celrep.2022.110617.

ACKNOWLEDGMENTS

We thank Guillaume Hucher, Esther Fournel, and Aurélie Daret for experimental help and support. We thank Isabelle Ferezou and Evan Harrell for advice. We thank ANR (Neurowhisk 14-CE24-0019, Mesobrain 20-CE37-0013, MotorSense 21-CE37-0012, iCODE, and NeuroSaclay 11-IDEX-0003-02),

FRM DEQ20170336761, CNRS|80Prime, FRC AAP2018, and the 3DS foundation.

AUTHOR CONTRIBUTIONS

D.E.S., L.E., and V.E.-S. initiated and supervised the project. H.L., D.G., D.E.S., L.E., and V.E.-S. designed the experiments. H.L. performed the experiments with help from D.G. H.L. analyzed the data with support from V.E.-S. and L.E. H.L. wrote the paper with inputs from all authors.

DECLARATION OF INTERESTS

The authors declare no competing interests.

Received: September 21, 2021
Revised: December 21, 2021
Accepted: March 14, 2022
Published: April 5, 2022

REFERENCES

Abbasi, A., Goueytes, D., Shulz, D.E., Ego-Stengel, V., and Estebanez, L. (2018). A fast intracortical brain–machine interface with patterned optogenetic feedback. J. Neural Eng. *15*, 046011.

Bathellier, B., Tee, S.P., Hrovat, C., and Rumpel, S. (2013). A multiplicative reinforcement learning model capturing learning dynamics and interindividual variability in mice. Proc. Natl. Acad. Sci. U S A *110*, 19950–19955.

Bosking, W.H., Sun, P., Ozker, M., Pei, X., Foster, B.L., Beauchamp, M.S., and Yoshor, D. (2017). Saturation in phosphene size with increasing current levels delivered to human visual cortex. J. Neurosci. *37*, 7188–7197.

Brecht, M. (2017). The body model theory of somatosensory cortex. Neuron *94*, 985–992.

Ceballo, S., Bourg, J., Kempf, A., Piwkowska, Z., Daret, A., Pinson, P., Deneux, T., Rumpel, S., and Bathellier, B. (2019a). Cortical recruitment determines learning dynamics and strategy. Nat. Commun. *10*, 1479.

Ceballo, S., Piwkowska, Z., Bourg, J., Daret, A., and Bathellier, B. (2019b). Targeted cortical manipulation of auditory perception. Neuron *104*, 1168–1179.e5.

Chen, X., Wang, F., Fernandez, E., and Roelfsema, P.R. (2020). Shape perception via a high-channel-count neuroprosthesis in monkey visual cortex. Science *370*, 1191–1196.

Choi, G.B., Stettler, D.D., Kallman, B.R., Bhaskar, S.T., Fleischmann, A., and Axel, R. (2011). Driving opposing behaviors with ensembles of piriform neurons. Cell *146*, 1004–1015.

Cuberovic, I., Gill, A., Resnik, L.J., Tyler, D.J., and Graczyk, E.L. (2019). Learning of artificial sensation through long-term home use of a sensory-enabled prosthesis. Front. Neurosci. *13*, 853.

Dadarlat, M.C., O'Doherty, J.E., and Sabes, P.N. (2015). A learning-based approach to artificial sensory feedback leads to optimal integration. Nat. Neurosci. *18*, 138–144.

Dalgleish, H.W., Russell, L.E., Packer, A.M., Roth, A., Gauld, O.M., Greenstreet, F., Thompson, E.J., and Häusser, M. (2020). How many neurons are sufficient for perception of cortical activity? ELife *9*, e58889.

Daniel, P.M., and Whitteridge, D. (1961). The representation of the visual field on the cerebral cortex in monkeys. J. Physiol. *159*, 203–221.

Dobelle, W.H. (2000). Artificial vision for the blind by connecting a television camera to the visual cortex. ASAIO J. *46*, 3–9.

Dobelle, W.H., Mladejovsky, M.G., and Girvin, J.P. (1974). Artificial vision for the blind: electrical stimulation of visual cortex offers hope for a functional prosthesis. Science *183*, 440–444.

El-Boustani, S., Sermet, B.S., Foustoukos, G., Oram, T.B., Yizhar, O., and Petersen, C.C.H. (2020). Anatomically and functionally distinct thalamocortical inputs to primary and secondary mouse whisker somatosensory cortices. Nat. Commun. *11*, 3342.

Estebanez, L., Férézou, I., Ego-Stengel, V., and Shulz, D.E. (2018). Representation of tactile scenes in the rodent barrel cortex. Neuroscience *368*, 81–94.

Fernández, E., Alfaro, A., Soto-Sánchez, C., Gonzalez-Lopez, P., Lozano, A.M., Peña, S., Grima, M.D., Rodil, A., Gómez, B., Chen, X., et al. (2021). Visual percepts evoked with an intracortical 96-channel microelectrode array inserted in human occipital cortex. J. Clin. Invest. *131*, e151331.

Flesher, S.N., Collinger, J.L., Foldes, S.T., Weiss, J.M., Downey, J.E., Tyler-Kabara, E.C., Bensmaia, S.J., Schwartz, A.B., Boninger, M.L., and Gaunt, R.A. (2016). Intracortical microstimulation of human somatosensory cortex. Sci. Transl. Med. *8*, 141–361.

Flesher, S.N., Downey, J.E., Weiss, J.M., Hughes, C.L., Herrera, A.J., Tyler-Kabara, E.C., Boninger, M.L., Collinger, J.L., and Gaunt, R.A. (2021). A brain-computer interface that evokes tactile sensations improves robotic arm control. Science *372*, 831–836.

Goueytes, D., Abbasi, A., Lassagne, H., Shulz, D.E., Estebanez, L., and Ego-Stengel, V. (2019). Control of a robotic prosthesis simulation by a closed-loop intracortical brain-machine interface. In 2019 9th International IEEE/EMBS Conference on Neural Engineering (NER) (IEEE), pp. 183–186.

Harding-Forrester, S., and Feldman, D.E. (2018). Somatosensory maps. Handb. Clin. Neurol. *151*, 73–102.

Hartmann, K., Thomson, E.E., Zea, I., Yun, R., Mullen, P., Canarick, J., Huh, A., and Nicolelis, M.A.L. (2016). Embedding a panoramic representation of infrared light in the adult rat somatosensory cortex through a sensory neuroprosthesis. J. Neurosci. *36*, 2406–2424.

Houweling, A.R., and Brecht, M. (2008). Behavioural report of single neuron stimulation in somatosensory cortex. Nature *451*, 65–68.

Huber, D., Petreanu, L., Ghitani, N., Ranade, S., Hromádka, T., Mainen, Z., and Svoboda, K. (2008). Sparse optical microstimulation in barrel cortex drives learned behaviour in freely moving mice. Nature *451*, 61–64.

Jiang, X., Shen, S., Cadwell, C.R., Berens, P., Sinz, F., Ecker, A.S., Patel, S., and Tolias, A.S. (2015). Principles of connectivity among morphologically defined cell types in adult neocortex. Science *350*, aac9462.

Kaas, J.H. (1997). Topographic maps are fundamental to sensory processing. Brain Res. Bull. *44*, 107–112.

Knutsen, P.M., Mateo, C., and Kleinfeld, D. (2016). Precision mapping of the vibrissa representation within murine primary somatosensory cortex. Philos. Trans. R. Soc. B Biol. Sci. *371*, 20150351.

Lashley, K.S. (1939). The mechanism of vision. XVI. The functioning of small remnants of the visual cortex. J. Comp. Neurol. *70*, 45–67.

Leal-Campanario, R., Delgado-Garcia, J.M., and Gruart, A. (2006). Microstimulation of the somatosensory cortex can substitute for vibrissa stimulation during Pavlovian conditioning. Proc. Natl. Acad. Sci. U S A *103*, 10052–10057.

Madisen, L., Mao, T., Koch, H., Zhuo, J., Berenyi, A., Fujisawa, S., Hsu, Y.-W.A., Garcia, A.J., Gu, X., Zanella, S., et al. (2012). A toolbox of Cre-dependent optogenetic transgenic mice for light-induced activation and silencing. Nat. Neurosci. *15*, 793–802.

Makin, T.R., and Bensmaia, S.J. (2017). Stability of sensory topographies in adult cortex. Trends Cogn. Sci. *21*, 195–204.

Merzenich, M.M., Knight, P.L., and Roth, G.L. (1975). Representation of cochlea within primary auditory cortex in the cat. J. Neurophysiol. *38*, 231–249.

Muller, L., Chavane, F., Reynolds, J., and Sejnowski, T.J. (2018). Cortical travelling waves: mechanisms and computational principles. Nat. Rev. Neurosci. *19*, 255–268.

Narayanan, R.T., Egger, R., Johnson, A.S., Mansvelder, H.D., Sakmann, B., de Kock, C.P.J., and Oberlaender, M. (2015). Beyond columnar organization: cell type- and target layer-specific principles of horizontal axon projection patterns in rat vibrissal cortex. Cereb. Cortex *25*, 4450–4468.

Nogueira, R., Rodgers, C.C., Bruno, R., and Fusi, S. (2021). The non-linear mixed representations in somatosensory cortex support simple and complex tasks. Preprint at bioRxiv. https://doi.org/10.1101/2021.02.11.430704.

O'Connor, D.H., Hires, S.A., Guo, Z.V., Li, N., Yu, J., Sun, Q.-Q., Huber, D., and Svoboda, K. (2013). Neural coding during active somatosensation revealed using illusory touch. Nat. Neurosci. *16*, 958–965.

O'Doherty, J.E., Lebedev, M.A., Ifft, P.J., Zhuang, K.Z., Shokur, S., Bleuler, H., and Nicolelis, M.A.L. (2011). Active tactile exploration using a brain–machine–brain interface. Nature *479*, 228–231.

Ortiz-Catalan, M., Mastinu, E., Greenspon, C.M., and Bensmaia, S.J. (2020). Chronic use of a sensitized bionic hand does not remap the sense of touch. Cell Rep. *33*, 108539.

Penfield, W., and Boldrey, E. (1937). Somatic motor and sensory representation in the cerebral cortex of man as studied by electrical stimulation. Brain *60*, 389–443.

Penfield, W., and Rasmussen, T. (1950). The Cerebral Cortex of Man; a Clinical Study of Localization of Function (Macmillan).

Peng, Y., Gillis-Smith, S., Jin, H., Tränkner, D., Ryba, N.J.P., and Zuker, C.S. (2015). Sweet and bitter taste in the brain of awake behaving animals. Nature *527*, 512–515.

Perronnet, L., Vilarchao, M.E., Hucher, G., Shulz, D.E., Peyré, G., and Ferezou, I. (2016). An automated workflow for the anatomo-functional mapping of the barrel cortex. J. Neurosci. Methods *263*, 145–154.

Rockland, K.S., Lund, J.S., and Humphrey, A.L. (1982). Anatomical banding of intrinsic connections in striate cortex of tree shrews (Tupaia glis). J. Comp. Neurol. *209*, 41–58.

Romo, R., Hernández, A., Zainos, A., and Salinas, E. (1998). Somatosensory discrimination based on cortical microstimulation. Nature *392*, 387–390.

Rosselet, C., Zennou-Azogui, Y., Escoffier, G., Kirmaci, F., and Xerri, C. (2008). Experience-dependent changes in spatiotemporal properties of cutaneous inputs remodel somatosensory cortical maps following skin flap rotation. Eur. J. Neurosci. *27*, 1245–1260.

Sachidhanandam, S., Sreenivasan, V., Kyriakatos, A., Kremer, Y., and Petersen, C.C.H. (2013). Membrane potential correlates of sensory perception in mouse barrel cortex. Nat. Neurosci. *16*, 1671–1677.

Schmidt, E.M., Bak, M.J., Hambrecht, F.T., Kufta, C.V., O'Rourke, D.K., and Vallabhanath, P. (1996). Feasibility of a visual prosthesis for the blind based on intracortical microstimulation of the visual cortex. Brain J. Neurol. *119*, 507–522.

Schofield, J.S., Shell, C.E., Beckler, D.T., Thumser, Z.C., and Marasco, P.D. (2020). Long-term home-use of sensory-motor-integrated bidirectional bionic prosthetic arms promotes functional, perceptual, and cognitive changes. Front. Neurosci. *14*, 120.

Tabot, G.A., Dammann, J.F., Berg, J.A., Tenore, F.V., Boback, J.L., Vogelstein, R.J., and Bensmaia, S.J. (2013). Restoring the sense of touch with a prosthetic hand through a brain interface. Proc. Natl. Acad. Sci. U S A *110*, 18279–18284.

Tabot, G.A., Kim, S.S., Winberry, J.E., and Bensmaia, S.J. (2015). Restoring tactile and proprioceptive sensation through a brain interface. Neurobiol. Dis. *83*, 191–198.

Vanni, M.P., Chan, A.W., Balbi, M., Silasi, G., and Murphy, T.H. (2017). Mesoscale mapping of mouse cortex reveals frequency-dependent cycling between distinct macroscale functional modules. J. Neurosci. *37*, 7513–7533.

Venkatraman, S., and Carmena, J.M. (2011). Active sensing of target location encoded by cortical microstimulation. IEEE Trans. Neural Syst. Rehabil. Eng. *19*, 317–324.

Vilarchao, M.E., Estebanez, L., Shulz, D.E., and Férézou, I. (2018). Supra-barrel distribution of directional tuning for global motion in the mouse somatosensory cortex. Cell Rep. *22*, 3534–3547.

Winawer, J., and Parvizi, J. (2016). Linking electrical stimulation of human primary visual cortex, size of affected cortical area, neuronal responses, and subjective experience. Neuron *92*, 1213–1219.

Woolsey, T.A., and Van der Loos, H. (1970). The structural organization of layer IV in the somatosensory region (S I) of mouse cerebral cortex: the description of a cortical field composed of discrete cytoarchitectonic units. Brain Res. *17*, 205–242.

Yizhar, O., Fenno, L.E., Davidson, T.J., Mogri, M., and Deisseroth, K. (2011). Optogenetics in neural systems. Neuron *71*, 9–34.

STAR★METHODS

KEY RESOURCES TABLE

REAGENT or RESOURCE	SOURCE	IDENTIFIER
Experimental models: organisms/strains		
Emx-cre X Ai27 transgenic mice	Madisen et al., 2012	Crossing RRID: IMSR_JAX:005628; RRID: IMSR_JAX:012567
Software and algorithms		
C++ Software Handling the behaviour	This paper	https://doi.org/10.5281/zenodo.6337587
Code used to analyze the data	This paper	https://doi.org/10.5281/zenodo.6337587
Intrinsic Imaging Software	This paper	https://doi.org/10.5281/zenodo.6337587
Other		
DLP, Vialux V-7001, 462 nm blue LED	Vialux	N/A
CCD camera (Basler acA640120 um)	Basler	N/A

RESOURCE AVAILABILITY

Lead contact

Further information and requests for resources should be directed to and will be fulfilled by the lead contact, Valérie Ego-Stengel (valerie.ego-stengel@cnrs.fr).

Materials availability

This study did not generate new material.

Data and code availability

- Data reported in this paper will be shared by the lead contact upon request.
- All original code has been deposited on GitHub and is publicly available as of the date of publication. The DOI is listed in the key resources table.
- Any additional information required to reanalyze the data reported in this paper is available from the lead contact upon request.

EXPERIMENTAL MODEL AND SUBJECT DETAILS

We used 6-week-old Ai-27 x EMX-Cre mice, expressing channelrhodopsin in excitatory neurons across the cortex (Madisen et al., 2012). Experimental procedures have been approved by the French Ministry of Research and Ethics Committee #59 as part of project #858-2015060516116339. A total of 14 mice (6 female, 8 male) were successfully implanted, water restricted, and then trained in the task. During the training period, mice only had access to water during the sessions as reward, and right after the session for supplementation whenever necessary.

METHOD DETAILS

Mouse preparation

Surgeries were performed on anesthetized mice (1%–4% isoflurane anesthesia in 100% air) placed on a regulated heating pad. The state of the anesthesia was assessed by breathing rate and response to tail pinch. The scalp was resected after lidocaine-induced local anesthesia (200 mg/L, 0.1 mL) and conjunctive tissues were removed. A head-post was glued (cyanoacrylate glue) to the skull, then strengthened with dental cement. A 5 to 6 mm diameter craniotomy was then performed while preserving the dura, centered either on the stereotaxic coordinates of the C2 barrel in the primary somatosensory cortex (P1.5-L3.3 mm), or on a more medial location in between the paw representation and the barrel cortex (P0.5-L2.3 mm). A glass optical window of diameter 5 or 6 mm was glued to the borders of the craniotomy. The remaining exposed skull was covered with dental cement. At the end of the surgery, we administrated subcutaneously an analgesic (2 mg/mL Metacam, 0.1 mL) and an antibiotic (2.4% Borgal, 0.2 mL). Intrinsic imaging sessions through the window were performed 5 to 10 days after the surgery. During an imaging session, either a single whisker or the right forepaw was stimulated with a piezoelectric bender (Physics Instruments) 100 Hz, 5 ms square wave deflection) while red light (625 nm) was projected on the window right below light saturation. A CCD camera acquired 659*494 px images at a rate of

60 fps. The images were analyzed for space-time fluctuations in luminescence (Optimage, Thomas Deneux, NeuroPSI). These intrinsic imaging sessions were used to locate the C2, Alpha and Delta barrel locations, as well as the forepaw location (Figures 1C and 4B). More details can be found in Abbasi et al., (2018).

Optogenetic photostimulation

During training, optogenetic stimulation was performed through the optical window (Figure 1A) using a Digital Light Processing module (DLP, Vialux V-7001, 462 nm blue LED. Stimulation patterns consisted of light bars 700 microns long and 150 microns wide, rotating on a disk of diameter 1.5 mm. This pattern was chosen as part of our interest in encoding the angle of a joint (Goueytes et al., 2019). The disk was centered on the C2 barrel location (vS1, Figure 1B, n = 11 mice). In three additional mice, the stimulation was centered on a point 1.5 mm medial and 1 mm rostral to the C2 barrel, thus on the trunk and legs representation (''body'' S1, bS1, Figures 4A and 4B). Among the 14 mice, four were subsequently trained with the stimulation centered on the posterior parietal cortex (PPC), 1.5 mm caudal to the C2 barrel (Figure 4A; three mice after vS1 training, one after bS1 training). To avoid overstimulation of cortical areas, the center of the stimulated disk was never illuminated (white spot in Figure 1D). Photostimulation was done at high power (measured, 10–15 mW per mm^2). Using a photodetector, we ensured that the edge of the photostimulation was sharp; intensity decreased to 5% at 20 microns from the edge. Spiking activity resulting from similar photostimulation was demonstrated previously (Abbasi et al., 2018; Ceballo et al., 2019b; Madisen et al., 2012). In pilot experiments, we checked that the particular light bar designed for this study also evoked spiking across the optical window. We conducted electrophysiological recordings with 1-shank electrodes (Neuronexus, 64-channel multisite extracellular electrode, A1x64-Poly2-6mm-23S-160) inserted obliquely through a small opening in the cranial window, while projecting patterns of light on S1 (Figure S1D). We typically performed several penetrations at different entry points along the anterior-posterior axis, thus exploring different parts of S1 and surroundings. Analysis of individual single-unit spike trains (Blackrock acquisition system, Spyking Circus) demonstrated strong neural activation by the optogenetic bar moving above the location of the recording site (Figure S1E). These results confirmed that optogenetic stimulation of neocortex in Emx-Cre x Ai27 mice induces neural activation (Ceballo et al., 2019b; Madisen et al., 2012).

Behavioral training

After surgery and intrinsic imaging, mice were water restricted. Training started two days later. During the first session, the mouse was habituated to head-fixation and learned to lick water from a small tube. During this session, licks always triggered water rewards, and nothing happened if the mouse did not lick. Each subsequent session lasted 30 min, during which a randomized set of trials was presented to the mouse. Trials were separated by 5 s.

In the standard condition, each trial consisted in the presentation of one trajectory of the photostimulation bar, starting from the most caudal position, and then rotating towards a rostral rewarded zone with different dynamics. The bar angular position was updated every 10 ms. Each trajectory was taken from a database of 252 pre-loaded trajectories. These were obtained from a closed-loop BMI study performed with different mice (Goueytes et al., 2019). In that study, the activity of motor cortex neurons was used to drive the rotating bar. From the initial full dataset, we kept only the 126 trajectories lasting between 10 and 20 s, entering at least once the rewarded zone (green zone, Figure 1E). To remove a possible right/left bias, for each trajectory, its symmetric trajectory with respect to the rostro-caudal axis was added to the database, yielding the full set of 252 smooth trajectories with evolving dynamics (Figures S1A–S1C).

A lick had different consequences depending on the angular location of the photostimulation bar at that time. A lick when the light bar was in the rewarded zone (green area, Figure 1E) led to an immediate 10 μL water reward. A lick in the no-lick zone (red area) immediately ended the trial and was followed by the 5 s intertrial interval, during which the cortex was not photostimulated. A new trial started immediately after the 5 s period. A lick in the neutral zones (white areas) had no consequence. If the mouse drank more than 3 mL of water during one session, only one lick out of two was rewarded with water during the following sessions, starting with the first lick inside the rewarded zone. The rewarded zone spanned 60°, except for three mice for which it spanned 50°.

Mice were trained for 5 to 10 daily sessions of 30 min each. Three mice initially trained for 5 days in the standard condition on vS1 were then trained for 5 days in a difficult condition, in which the size of the no-lick zone was increased so that the task became more challenging (Figure S4, these were the three mice trained with a 50° rewarded zone). Three other mice were also initially trained in the standard condition and were then tested for one session in a shuffled condition (Figures 2A–2F), in which the contiguity of the cortical sectors crossed during the trajectories was modified. Specifically, the stimulation disk was divided in six 60° sectors, and these sectors were swapped so that the trajectory jumped from one sector to another at the boundaries. The starting position and rewarded zone were unchanged. Another group of three naive mice were directly trained in the shuffled condition on vS1 (Figures 2B–2E).

Mice were usually trained every day for 10 days once enrolled in a protocol. However, in the first experiments, training was often stopped after 5 days of vS1 stimulation in the standard condition because the performance of the mice was already very high. When training duration varied across mice, the last session of each mouse was labelled Last for group analysis.

Histology

After training, mice were deeply anesthetized with isoflurane (4%–5%), euthanized by cervical dislocation, and perfused with paraformaldehyde (PFA). The brains were stored in PBS for two days or more, and then S1 tangential slices (100 microns thick) were cut and stained with cytochrome C oxidase. The alignment of the stained barrels and the blood vessels were computed using a

homemade software (Perronnet et al., 2016). Briefly, this software uses the position of the transversal vessels to realign each slice with respect to each other. At the end of the process, the slice showing the blood vessels on the surface of the cortex and the slices showing the stained barrels could be superimposed accurately (Figure 1D).

QUANTIFICATION AND STATISTICAL ANALYSIS

We quantified performance by assessing the percentage of trials that were rewarded in each session. We also computed a detection value (Figure 1G), corresponding to the percentage of entries into the rewarded zone for which the mouse obtained at least one reward. Therefore, the detection value was not affected by trials that were interrupted before reaching the rewarded area. Overall, a high detection value indicates that the mouse learned to lick when the light bar was in the rewarded zone, while a high percentage of rewarded trials requires that in addition, the mouse learned to refrain from licking in the no-lick zone. These two measures of performance were normalized session by session by estimating a chance level obtained by bootstrapping. For each session, one hundred shuffled sessions were generated by loading random sequences of trajectories from the database while keeping the temporal sequence of licks from the real session. The simulated protocol followed all the task rules: if during a simulated trajectory, a lick happened while photostimulation was in the no-lick zone, a 5 s intertrial interval was enforced and a new trial was loaded thereafter. The average performance of these simulations was then subtracted from the performance of the real session to obtain the normalized performance (Figures 1G, 2B, 3C, and 3D).

To demonstrate that mice were using spatial information from the cortical stimulus and not only a temporal strategy, we designed an algorithm that solves the task exclusively by using time elapsed from the start of the trial. In the simplest version, this algorithm waits a fixed amount of time, called its operating time, then licks continuously until the end of the trial. In the version we used, instead of a fixed value, we picked waiting times randomly from a Gaussian distribution centered on the operating time, and with a standard deviation equal to the smallest standard deviation of response times observed in a trained mouse. We generated one such algorithm for each operating time from 0 to 20 s (with 0.01 s steps). For each operating time, we quantified the performance of the algorithm by the detection value and percentage of rewarded trials for a full session comprised of the 252 different trials.

To quantify the behavioral licking response of the mice as a function of cortical location, we analyzed the distribution of angular positions of the optogenetic bar at lick times (Figures 2A–2C). However, as a lick in the rewarded zone leads to a reward and thus to more licks, these plots often showed large numbers of licks not necessarily linked to the simultaneous photostimulation location. To disambiguate first licks from others, we defined an onset lick as a lick that was not preceded by another lick in the last 3 s.

Each statistical test used is described in the text and/or in the figure legends. *: $p < 0.05$. **: $p < 0.01$. ***: $p < 0.001$.

Cell Reports, Volume *39*

Supplemental information

Continuity within the somatosensory cortical map facilitates learning

Henri Lassagne, Dorian Goueytes, Daniel E. Shulz, Luc Estebanez, and Valerie Ego-Stengel

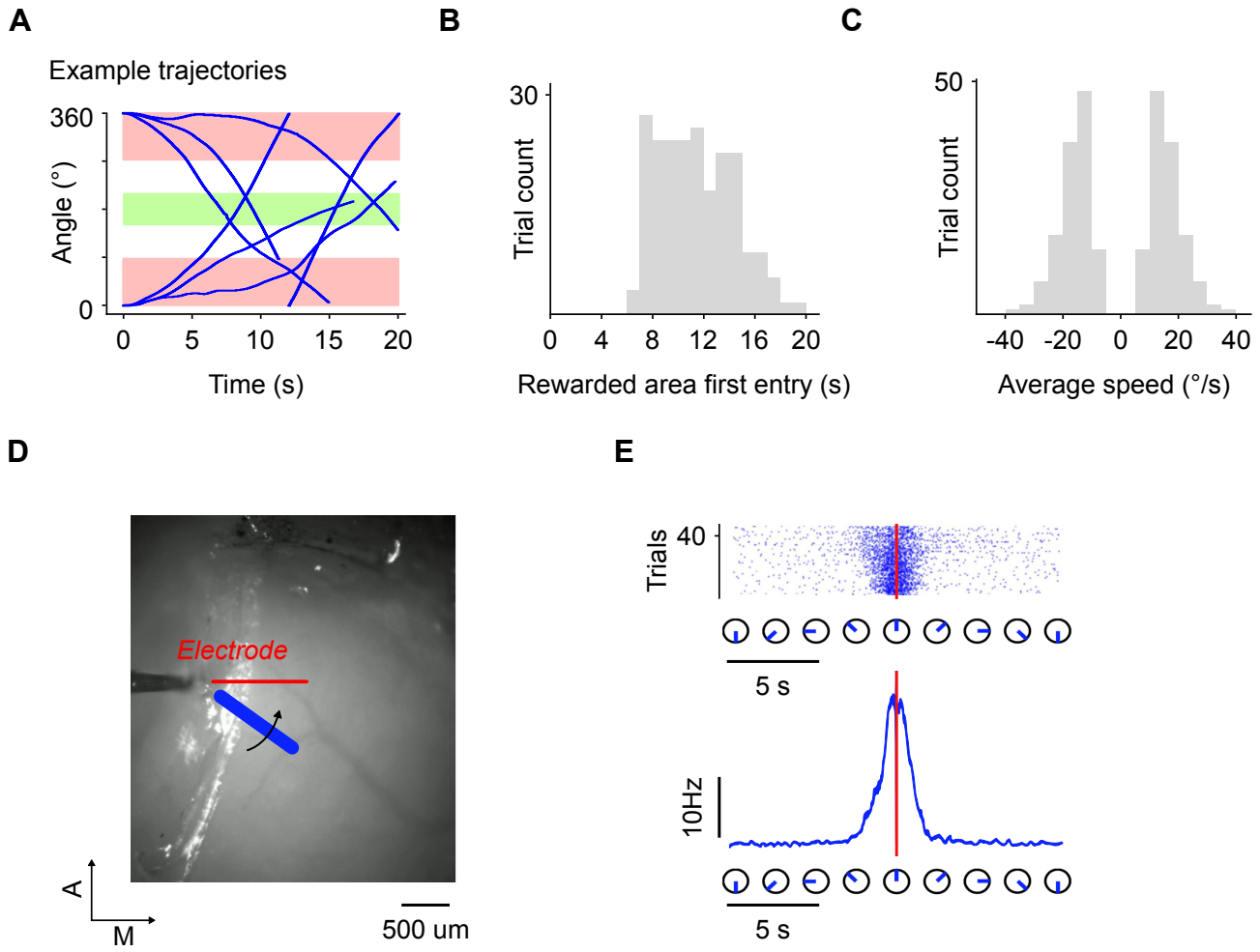

Figure S1. Optogenetic task dynamics and neural activation. Related to Figure 1.

(A) Six example trajectories of the optogenetic stimulation. The reference angle 0° corresponds to the angle for the lowest point on Figure 1E, most posterior on the cortical surface. The photostimulation bar could rotate several times around the center, and could reverse directions.

(B) Distribution of the times of first entry of the optogenetic stimulation in the Rewarded zone, for the 252 trajectories in the database.

(C) Distribution of the average angular speed of the optogenetic stimulation, for the 252 trajectories in the database. The bar can move either clockwise or counterclockwise.

(D) Recordings in S1 with a silicon longitudinal multi-site electrode (Neuronexus, 64-channel multisite extracellular electrode, A1x64-Poly2-6mm-23S-160), while stimulating the cortex with a moving optogenetic bar. Here the bar is of same width but longer than for the behavioral task, so that we could ensure that it passes over most electrode sites. The red line indicates the electrode shank in the brain.

(E) Top: Example raster plot of spikes from a single unit as the optogenetic bar rotates, demonstrating strong activation.

Bottom: Peri-Stimulus Time Histogram of the same spiking activity.

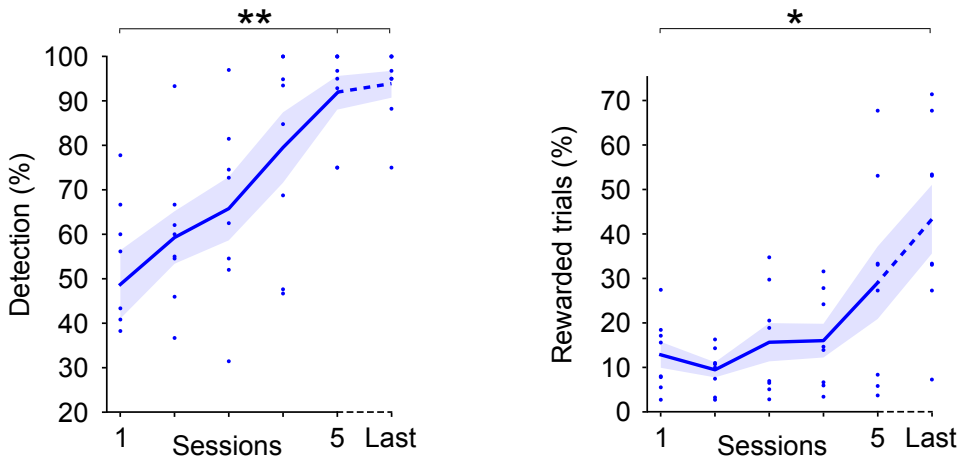

Figure S2. Raw Learning curves. Related to Figure 1.

Learning curves as in Figure 1G, but before subtracting the chance level calculated by bootstrapping the trials for each individual session (see Methods)

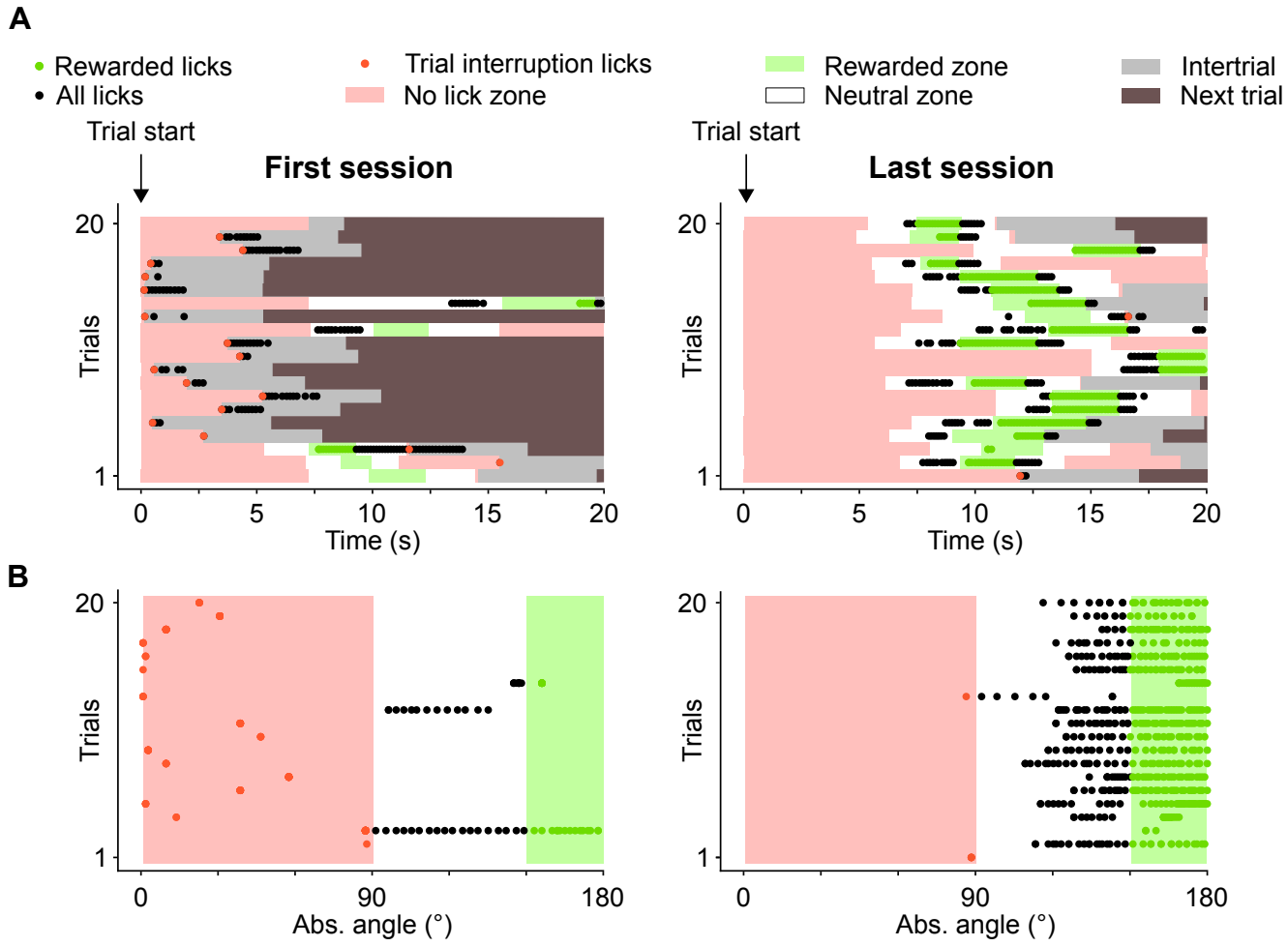

Figure S3. Mice learn to lock their licking behavior to the stimulation angle in cortical space. Related to Figure 1.

(A) Raster plots of licks (dots) as a function of time after trial onset, during 20 consecutive trials in the first and tenth session for one mouse. Same graphs as Figure 1F.

(B) Raster plots similar to Panel A, but as a function of the absolute angle of the photostimulation bar on the cortical surface. The reference angle 0° corresponds to the lowest point of Figure 1E, most posterior on the cortical surface. Angles were mapped to [-180°,180°] before taking the absolute value. Note that because the horizontal axis represents angles, licks on the right do not necessarily happen before licks on the left.

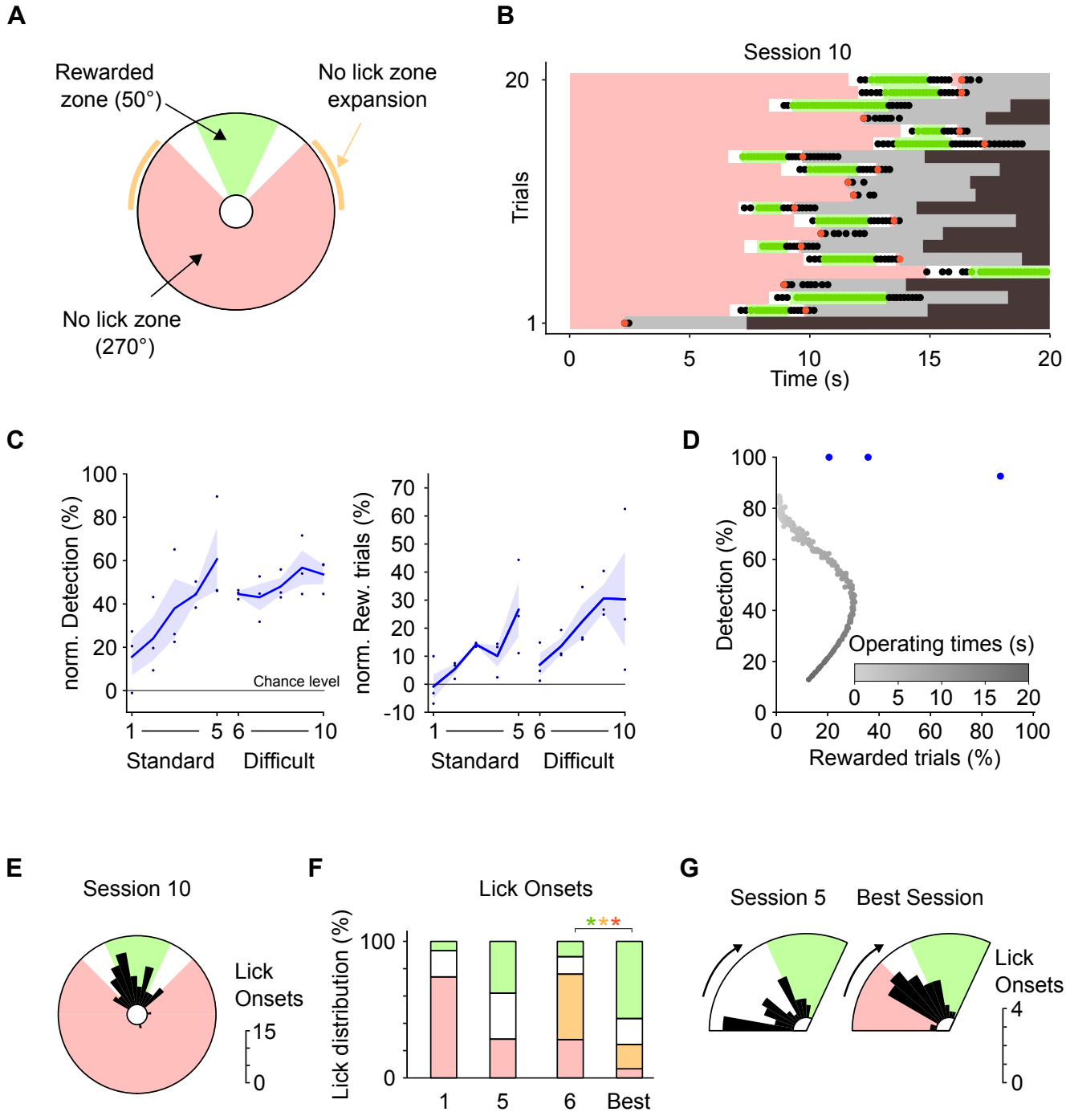

Figure S4. Mice finely discriminate spatial zones of stimulation. Related to Figure 2.

(A) In the difficult condition, the no-lick zone was expanded from 180° to 270° while the neutral zones were each reduced from 60° to 20°. Orange lines: expanded area of the no-lick zone.

(B) Raster plot of licks (dots) during the first 20 trials of the last session of a mouse trained on the difficult task for 5 days, after having been trained on the standard task for 5 days. Conventions are the same as for Figure 1F. Lick onsets largely occur in the neutral and rewarded zones.

(C) Average learning curves (+/- SEM, n = 3 mice), quantified by the normalized detection level (Left), and the normalized percentage of rewarded trials (Right).

(D) Performance curve of an algorithm solving the difficult condition task with a pure temporal strategy (see Methods and Figure 1H). The blue dots indicate the mice performance during their last session.

(E) Spatial distribution of the optogenetic stimulus angle for lick onsets for the session shown in panel B.
(F) Average distribution of lick onsets for which the optogenetic bar was in the rewarded, no-lick and neutral zones, for the first and last (or best) session of the two training conditions. Orange corresponds to licks in the no-lick expansion zone. Best session corresponds to each mouse's highest performance among session 9 and session 10. This adaptation of the quantification was necessary because the task was very challenging, so performance was highly variable.
(G) Average spatial distribution of the stimulus angle for lick onsets for the neutral and rewarded zones. Trials entering from the right were symmetrized before averaging as for Figure 2C. Only the first 20 rewarded trials of a given session were used for this analysis, ensuring that the mice were highly motivated.